

*To appear in Journal of Statistical Physics*

## 2D Crystal Shapes, Droplet Condensation and Exponential Slowing Down in Simulations of First-Order Phase Transitions

Thomas Neuhaus<sup>1</sup> and Johannes S. Hager<sup>2, 3</sup>

*Version of March 22, 2022*

---

Multicanonical ensemble simulations for the simulation of first-order phase transitions suffer from exponential slowing down. Monte Carlo autocorrelation times diverge exponentially with free energy barriers  $\Delta F$ , which in  $L^d$  boxes grow as  $L^{d-1}$ . We exemplify the situation in a study of the 2D Ising-model at temperature  $T/T_c = 0.63$  for two different lattice manifolds, toroidal lattices and surfaces of cubes. For both geometries the effect is caused by discontinuous droplet shape transitions between various classical crystal shapes obeying geometrical constraints. We use classical droplet theory and numerical simulations to calculate transition points and barrier heights. On toroidal lattices we determine finite size corrections to the droplet free energy, which are given by a linear combination of Gibbs-Thomson corrections, capillary wave fluctuation corrections, constant terms and logarithmic terms in the droplet volume. Tolman corrections are absent. In addition, we study the finite size effects on the condensation phase transition, which occurs in infinite systems at the Onsager value of the magnetization. We find that this transition is of discontinuous order also. A combination of classical droplet theory and Gibbs-Thomson corrections yields a fair description for the transition point and for the droplet size discontinuity for large droplets. We also estimate the nucleation barrier that has to be surmounted in the formation of the stable droplet at coexistence.

---

**Key Words:** Nucleation, Ising model, Multicanonical simulations, geometric phase transitions.

---

<sup>1</sup>Finkenweg 15, D – 33824 Werther, Germany; e-mail: neuhaus@rock.helsinki.fi.

<sup>2</sup>Institute for Physical Science and Technology, University of Maryland, College Park, Maryland 20742.

<sup>3</sup>Present address: Fachbereich Physik, Universität Essen, D-45117 Essen, Germany; email: johannes@theo-phys.uni-essen.de

## 1. INTRODUCTION

First-order phase transitions play an important role in many branches of physics ranging from the well known liquid vapor transition <sup>(1,2)</sup> to nuclear physics <sup>(3)</sup>, protein folding <sup>(4)</sup> or even to the symmetry breaking in the early universe <sup>(5)</sup>. Even for the intensely studied liquid vapor transition there are still considerable uncertainties in the calculations of the decay rate of metastable states <sup>(1)</sup>, partially due to unknown finite size and finite curvature corrections to the free energy and the surface tension of droplets.

The present study uses the two dimensional Ising-model to investigate the influence of such finite size effects, because it is conceptually simple and there is a large body of rigorous results, which can be used in the comparison to simulation data. The partition function of the Ising-model is given by

$$Z = \sum_{conf.} e^{-\beta H} \quad , \quad (1.1)$$

with the Hamiltonian

$$H = H_I - hM := - \sum_{\langle i,j \rangle} s_i s_j - h \sum_i s_i \quad , \quad (1.2)$$

where  $H_I$  contains the usual nearest neighbor interaction and the magnetization  $M$  couples linearly to a external magnetic field  $h$ . We use the multicanonical sampling method to study the model in the whole magnetization interval  $[-L^2, L^2]$  at the inverse temperature  $\beta = 0.7$  (corresponding to  $T/T_c = 0.63$ , with  $\beta_c = \ln(1 + \sqrt{2})/2$ ), which is sufficiently low to pronounce effects due to first-order phase transitions, but still high enough to use a isotropic surface free energy as a good first approximation. Most of our efforts will be focused on the magnetic probability distribution

$$P_L(M) = \frac{1}{Z} \sum_{conf.} e^{-\beta H} \delta(M - \sum_i s_i) \quad , \quad (1.3)$$

which up to a normalization factor equals the restricted partition function  $Z(m, L)$ . The distribution  $P_L(M)$  was already studied in <sup>(6,7,8,9)</sup> with the aim to understand the dynamics of the decay of a metastable state. Our goal in this paper is to produce a quantitative description for high resolution Monte-Carlo data of  $P_L(M)$  in terms of classical droplet theory, including the leading finite-size effects.

The paper is organized as follows. In section 2 we give a brief review of the multicanonical sampling method and present numerical evidence of residual exponential slowing down, due to the singularities associated with

first order phase transitions. We argue that similar limitations are present in other broad histogram sampling methods. In section 3 we present the classical theory for the boundary induced geometric phase transitions in toroidal and cube-surface geometries. Section 4 discusses the influence of a variety of possible finite size effects. Section 5 gives a detailed account of our simulation data for both geometric phase transitions and the droplet condensation transition, including the analysis of finite size effects. In section 6 we conclude our findings.

## 2. MULTICANONICAL METHOD

Multicanonical (Muca) sampling was invented <sup>(10,11)</sup> to eliminate the exponential slowing down of canonical (Metropolis or heat bath) simulations near temperature- or field-driven first-order phase transitions. At inverse temperatures  $\beta > \beta_c$  the magnetic probability distribution  $P_L(M)$  as a function of the magnetization  $M$  in the Ising-model has two maxima, which we denote by  $\pm M_L^{max}$ , separated by a valley, where the probability is suppressed by a factor  $e^{-\Delta F}$ , due to the additional free energy  $\Delta F \sim \sigma L$  of the interface present in the two phase region. Already for moderate system sizes canonical simulations are not able to sample these exponentially suppressed states and the simulation gets trapped in one of the maxima of  $P_L(M)$ . Similar problems arise in simulations of spin glasses. The Muca method remedies this issue by biasing the sampling with a weight factor  $P_L(M)^{-1}$ , thereby producing flat histograms <sup>(12,13)</sup>. Alternatively one can use the inverse of the density of states  $n(E)^{-1}$  for a given internal energy  $E$  to enhance the sampling of the suppressed states in energy driven first order phase transitions. Thus the simulations are performed with an effective Hamiltonian  $H_{eff} = H_I + \beta^{-1} \ln P_L(M)$ . Unbiased averages can be calculated via

$$\langle A \rangle = \frac{\sum_{conf.} A e^{-\beta(H_I - H_{eff})}}{\sum_{conf.} e^{-\beta(H_I - H_{eff})}} \quad . \quad (2.1)$$

A major practical problem in the application of the method is, that one needs a fairly good approximation of  $P_L(M)$  to run a efficient Muca simulation. The determination of an estimate for  $P_L(M)$  by conventional importance sampling may consume already large parts of the overall computation time, especially for systems with a rough energy landscape, like spin-glasses. Recursive schemes have been proposed <sup>(14)</sup> for the cases where finite size scaling cannot be used to extrapolate  $P_L(M)$  to large system size  $L$ . Recently several new ideas which tackle this practical problem by forcing the simulation into the unfavorable states have been put forward <sup>(15,16)</sup>.

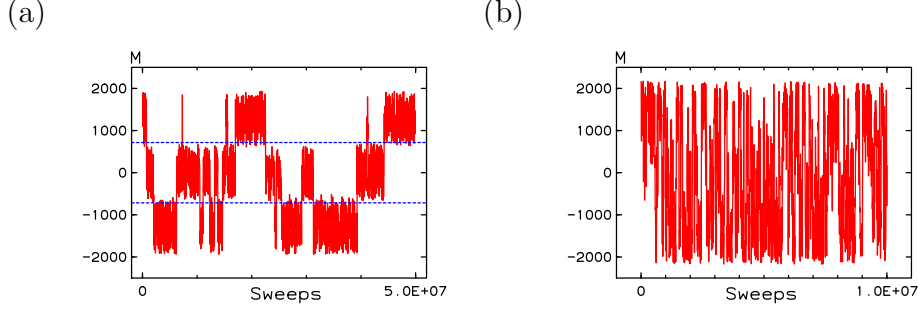


Figure 1: (a) Time series for magnetizations  $M$  in Muca simulations at  $\beta = 0.7$  on a toroidal  $44^2$  lattice as compared to (b) time series for  $M$  on a cube-surface SH(20) lattice, which has a similar volume. The statistics is  $5 \cdot 10^7$  sweeps on the torus and  $10^7$  sweeps on the SH lattice. The horizontal lines for the torus indicate the position of shape transitions.

We now want to focus on the performance of the algorithm, supposing we have the exact probability distribution  $P_L(M)$  at hand. For this purpose we study the system size dependence of the autocorrelation time  $\tau$ , defined as the mean time needed by the algorithm to go from the left side of the magnetization range at  $-M_L^{max}$  to the right one at  $M_L^{max}$  and back again. After transforming away the energy barrier due to the interface we may at best expect a random walk motion of the algorithm in the magnetization. A walk between  $-M$  and  $M$  then takes  $O(M^2)$  spin flips. With  $M \sim L^2$  and the usual definition of Monte-Carlo time in units of  $L^2$  attempted spin flips (sweeps) we arrive at  $\tau \sim L^2$  for the optimal behavior of  $\tau(L)$ . The sobering news of Fig. 1 – displaying time series for the magnetization  $M$  in Muca simulations of the 2D Ising-model at inverse temperature  $\beta = 0.7$  on a torus and a cube-surface (see Fig. 5) – is, that the assumption of random walk like motion in the whole magnetization interval is plainly wrong. For the torus geometry (pbc.) one clearly sees that the interval for the magnetization at least is divided into three sectors with random walk like behavior, separated by two barriers. For the cube-surface, which we abbreviate in the sequel as SH (for surface of a hypercube in case  $d > 2$ ), the presence of barriers is less obvious. An estimate of the magnitude of barriers can be obtained, if  $\tau$  is fitted with the form

$$\tau = A_\tau V e^{R\sigma\partial\Omega_{max}}, \quad (2.2)$$

where the maximal surface  $\partial\Omega_{max}$ , which determines the exponential slowing down, is  $2L$  on a toroidal  $L^2$  box and  $4(L-1)$  on a  $SH(L)$  lattice. The symbol  $\sigma$  denotes the surface tension and  $V$  is the volume. We obtain

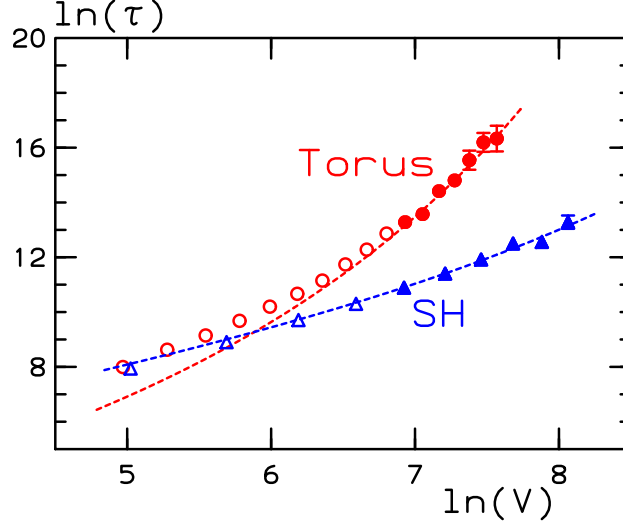


Figure 2: Multicanonical autocorrelation times  $\tau$  for the torus (circles) and SH lattices (triangles) in the 2D Ising-model at  $\beta = 0.7$  in units of heatbath sweeps as a function of the box volume  $V$ . The plot is double logarithmic. Curves are explained in the text.

the values

$$R = 0.121(14) \quad \text{Torus} \quad (2.3)$$

$$R = 0.031(05) \quad \text{SH} \quad , \quad (2.4)$$

from the fits as displayed in Fig. 2. Into the fit enter data, which in the figure are displayed with solid symbols. The measured  $R$ -values are significantly smaller than values  $R \approx 1$  as expected for non multicanonical simulations, but clearly indicate the presence of residual exponential slowing down. We show, that the barrier on the torus, which leads to a exponential slowing down, is caused by a geometrically induced first-order transition from a droplet to a strip domain, whose barrier value can be calculated using classical droplet theory. The droplet theory result  $R = 0.1346\dots$  agrees within error bars with the measured value of (2.3). A superficial inspection of the time series for the cube-surface, see Fig. 1b, might lead to the guess, that in this case no barriers are present. We will show, that in this case there is a series of three different discontinuous transitions in-between phase space regions, where droplets occupy one, two, three and four corners on the cube-surface. The barrier values are

$R_{1/2} = 0.02987$ ,  $R_{2/3} = 0.02977$  and  $R_{3/4} = 0.03441$ , which all are smaller than corresponding barriers on the torus and, the maximum value  $R_{3/4}$  again agrees within error bars with the measured value cited in (2.4).

Now, as already pointed out by Leung and Zia <sup>(17)</sup>, one could avoid this type of geometrical phase transitions by simulating the Ising-model on the surface of a sphere, and actually the cube-surface may be viewed as a crude approximation to the sphere. Alas there is no way known to put a regular lattice of arbitrary volume on the surface of a sphere, but off lattice simulation of liquid-gas systems could do the job. Are we then able to achieve random walk like Muca dynamics in the whole interval of magnetizations? Our answer to this question still is no, since there is an additional first-order transition present, namely the droplet condensation phase transition from a uniform one phase region to the phase separated two phase region, where we have yet another essential singularity in the free energy. Here again we find a, albeit much smaller barrier for the Muca simulations, which is now directly related to the physical nucleation barrier associated with the formation of a critical nucleus <sup>(18,19)</sup>. Now, what at first sight just looks like an embarrassing limitation of the algorithm, at a second thought gives us interesting information about the droplet condensation phase transition. In the quantitative analysis of this data Gibbs-Thomson corrections and other finite size effects will play a prominent role, since the volume of the coexisting droplet scales for large system sizes asymptotically as  $L^{4/3}$  and thereby introduces an additional scale. Our findings not only are relevant for the algorithmic performance of Muca simulations, but most likely limit the performance of other broad histogram methods – like the recently introduced Wang and Landau density of states sampling method<sup>(15)</sup> – as well, provided the Monte-Carlo covers a portion of phase space, which contains one of the mentioned singularities. For purposes of illustration we display in Fig. 3 the magnetization density time series obtained from a Wang-Landau broad histogram sampling in the magnetization of the 2D Ising-model on a  $400^2$  lattice at  $\beta = 0.7$ . The value of the Wang-Landau parameter  $f$  is  $f = 1.00007$  and the magnetization density of states is updated with a heat bath algorithm. The horizontal lines in the figure denote the Onsager value  $m_0$  and the position  $m_{cond}$  of the droplet condensation phase transition. The existence of a barrier is indicated by the presence of flip flops between two different regions of the phase space, below and above  $m_{cond}$ . This exponential slowing down worsens, if either lattice sizes are increased, or  $f$  is tuned to the value unity.

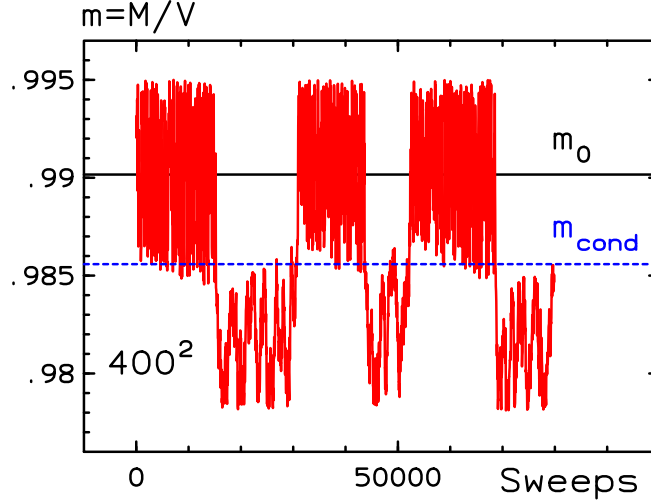


Figure 3: Time series for magnetization densities  $m$  in Wang-Landau density of states simulations at  $\beta = 0.7$  on a toroidal  $400^2$  lattice and at  $f = 1.00007$ . The simulation slows down at the position of the droplet condensation phase transition  $m_{cond}$ , which we study in the present paper.

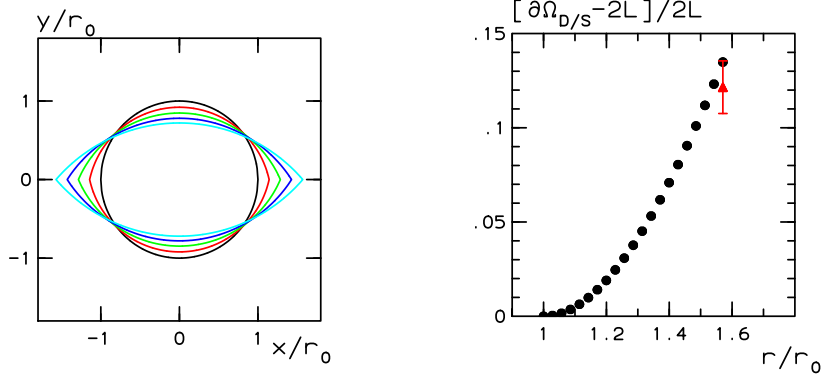
### 3. CLASSICAL DROPLETS

Below the critical point the bulk density of the spontaneous magnetization  $m_0(T)$  in a infinite system is given by Onsagers solution <sup>(20)</sup>, which at  $\beta = 0.7$  predicts the value  $m_0 = 0.99016\dots$  for the magnetization density. If we restrict the mean density of the magnetization to some value in the interval  $[-m_0, m_0]$  the system separates into two phases with magnetizations  $\pm m_0(T)$  divided by an interface. The orientation dependent free energy of a interface can be obtained from the spin-spin correlation function via a dual transformation <sup>(21)</sup>. The equilibrium shape of a droplet with volume  $\Omega$  of the minority phase, embedded in the majority phase, can be obtained by the celebrated Wulff construction <sup>(22)</sup>. The total free energy of the droplet is given by <sup>(17)</sup>

$$\Sigma_D = 2\sqrt{W\Omega} \quad (3.1)$$

where

$$W = \frac{4}{\beta^2} \int_0^{\beta\sigma_0} dx \cosh^{-1} \left[ \frac{\cosh^2(2\beta J)}{\sinh(2\beta J)} - \cosh(x) \right] \quad (3.2)$$



(a)

(b)

Figure 4: (a) Crystal shapes at the droplet strip transition. With the droplet volume fixed at its value  $L^2/\pi$  at coexistence the circular stable droplet is deformed into the unstable saddle point lens shaped droplet. (b) The percentile increase of the excess length  $(\partial\Omega_{D/S} - 2L)/2L$  as a function of the half base length  $r/r_0$  in units of  $r_0$ . At  $r/r_0 = \pi/2$  one reaches the saddle point configuration. The measured data point of (2.4) is plotted with error bars and agrees with the classical droplet result.

is the volume bounded by the Wulff plot of the orientation dependent surface free energy, and  $\sigma_0(T) = 2J + \frac{1}{\beta} \ln \tanh \beta J$  is the free energy of the  $(1,0)$  surface, which at  $\beta = 0.7$  has the value  $\sigma_0 = 0.89643\dots$ . In the presence of boundaries different equilibrium shapes can occur<sup>(23,24)</sup>. In the case of a torus with periodic boundary conditions there is a first-order phase transition from the droplet shape - as given by the Wulff construction - to a strip with surface free energy  $\Sigma_S = 2\sigma_0 L$ . The strip is wrapped around the torus and the transition point is determined by the condition  $\Sigma_D = \Sigma_S$ . This was shown rigorously by Shlosman<sup>(25)</sup>. Employing numerical integration for the integral in Eq. (3.2) one can precisely calculate the transition point  $m_{D/S}(T)$ , which at  $\beta = 0.7$  has the value

$$m_{D/S} = 0.36974\dots \quad (3.3)$$

In our Monte-Carlo data the transition is rounded and shifted due to several finite size effects, which will be discussed in detail in the next section. For the toroidal and cube-surface geometry we calculate in the rest of this section classical equilibrium shapes and saddle point configurations,



which determine transition points and barrier heights in-between the different phases. For sake of simplicity we use a isotropic surface free energy, which is still a reasonable approximation at inverse temperature  $\beta = 0.7$  ( $T/T_c = 0.63$ ), where the Monte-Carlo simulations are performed.

Toroidal boxes of linear extent  $L$  with periodic boundaries have a volume  $V = L^2$  and without boundaries the equilibrium droplet shape is just a circle of radius  $r = \sqrt{\Omega/\pi}$ , since it minimizes the surface  $\partial\Omega = \sqrt{4\pi\Omega}$  for a given volume  $\Omega$ . Leung and Zia<sup>(17)</sup> argued, that the saddle point configuration at the transition is a lens shaped droplet - see Fig. 4a - formed by two arcs with a base length  $L$ . At the transition point  $m_{D/S}/m_0 = 1 - 2/\pi$  this droplet interpolates in-between a spherical droplet of radius  $r_0 = L/\pi$  and the strip. The arc shape again follows from the minimization of the surface at given droplet volume  $L^2/\pi$ . Figure 4b displays the excess length of the droplet, which is deformed from its spherical shape at  $r/r_0 = 1$  to the lens shaped saddle point configuration with half base length value  $r/r_0 = \pi/2$ . The excess surface of the saddle point configuration is<sup>(17)</sup>

$$\frac{\partial\Omega_{D/S} - 2L}{2L} = 0.1346... \quad (3.4)$$

and we can directly check this value in our Muca simulations, since this barrier gives the leading exponential contribution to the autocorrelation time and should equal  $R$  of (2.3). The value of the classical excess length is in fair agreement with the simulation value. Some deviations may come from the influence of the anisotropy of the surface free energy, which at  $\beta = 0.7$  shifts the location of the transition by a few percents. Cube-surface lattices of parameter value  $L$  are 2D lattice manifolds denoted  $SH(L)$ , which are identified with the surface of a 3D cube with linear extend  $L - 1$ . An example is displayed in Fig. 5, where a  $SH(5)$  lattice with linear extent 4 is represented schematically. A  $SH(L)$  lattice has a volume  $V = 6(L - 2)^2 + 12(L - 2) + 8$  and there are eight sites on the corners of the cube, which possess three nearest neighbors instead of four. A classical droplet configuration at magnetization  $M = 0$  covers four of the eight corners and has a minimal surface of length  $\partial\Omega = 4(L - 1)$  separating spin up and spin down domains. A small droplet can lower its surface by occupying a corner of the cube. With increasing volume it becomes favorable to cover two, three and four corners and similar as on the torus there exist shape transitions in-between states, which occupy one, two, three and four corners. Due to our choice of a isotropic surface free energy all equilibrium droplet shapes consist out of circle segments, which are closed around the corners. To systematize our considerations we denote the uniquely defined circle segment of volume  $\Omega$  and base length  $b$

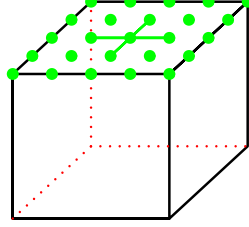


Figure 5: The  $SH(5)$  lattice manifold is identified with the surface of a  $5^3$  cubic box with linear extent 4.

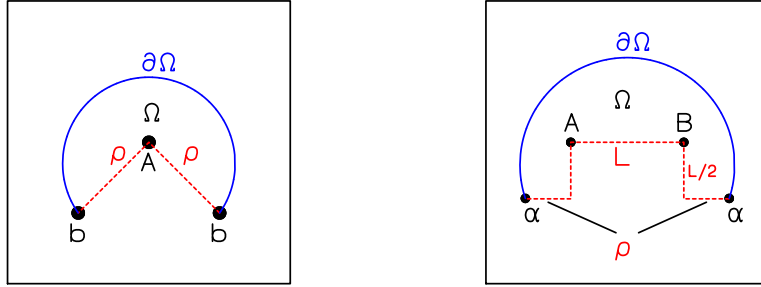
by  $S(b, \Omega)$  and its arc length by  $\partial\Omega(b, \Omega)$ . A droplet located at a corner has the volume  $\Omega_1 = \Omega[S(b, \Omega)] - b^2/4$  and the surface  $\partial\Omega_1 = \partial\Omega(b, \Omega)$ . Note that the base length itself does not contribute to the surface  $\partial\Omega(b, \Omega)$  of the droplet. The situation is depicted schematically in Fig. 6a, where the droplet covers the corner  $A$  and the base length has the value  $b = \sqrt{2}\rho$  with  $\rho$  as denoted in the figure. To get the equilibrium shape at constant volume  $\Omega_1$  we minimize  $\partial\Omega_1$  with respect to  $b$ . This results in

$$\partial\Omega_1 = \sqrt{3\pi\Omega_1} \quad (3.5)$$

as compared to  $\partial\Omega = \sqrt{4\pi\Omega}$  for a face centered droplet. Similar considerations apply to two corner droplets and Fig. 6b displays a droplet, which covers two corners  $A$  and  $B$ . The base length  $b$  has the value  $b = L + 2\rho$ , again with  $\rho$  as denoted in the figure. For the non-extremal droplet we have  $\Omega_2 = \Omega[S(b, \Omega)] - L^2/2$  and  $\partial\Omega_2 = \partial\Omega(b, \Omega)$ , which again after minimizing  $\partial\Omega_2$  with respect to  $b$  leads to the surface length

$$\partial\Omega_2 = \sqrt{\pi(2\Omega_2 + L^2)} \quad (3.6)$$

for the two corner equilibrium droplet of volume  $\Omega_2$ . Equating the surfaces (3.5) and (3.6) we find  $\Omega_{1/2} = L^2$  for the droplet volume  $\Omega_{1/2}$ , where the transition from the one corner to the two corner droplet occurs. To



(a)

(b)

Figure 6: Generic droplet shapes on SH lattice for (a) one corner and (b) two corner droplets. Capital letters denote sites on the corners of the SH lattice, small letters denote sites on the edges of the cube and greek letters denote sites neither located on edges or corners. Solid lines of the shapes contribute to the surface  $\partial\Omega$ , broken lines do not. Sites labeled with the same letter are to be identified.

calculate the barrier height at the transition we argue, that the saddle point configuration between the one corner and the two corner droplet is reached, when the site  $b$  of Fig. 6a occupies an additional corner: the site  $B$  of Fig. 6b. The volume of this droplet is  $\Omega_{1/2}$  and its surface has the value  $\partial\Omega_{1/2} = \partial\Omega(b = \sqrt{2}L, 3/2L^2)$ , leading to a excess length

$$\frac{\partial\Omega_{1/2} - \partial\Omega_1}{4L} = 0.02987 \quad (3.7)$$

normalized with the length  $4L$  of the “strip” or four corner droplet. Besides this transition we find two more, from the two corner to the three corner droplet and from the three to the four corner droplet. To parameterize the possible shapes of a three corner droplet we introduce the parameter  $s = \overline{Ad}/L$  as indicated in Fig. 7. We read of the volume of the three corner droplet

$$\Omega_3 = \Omega[S(b = L\sqrt{(3+s)^2 + (1-s)^2}, \Omega)] + L^2(1 - \frac{1}{2}(1-s)(3+s)) \quad (3.8)$$

and the surface of the droplet is again the arc length  $\partial\Omega_3(b(s), \Omega)$ . Numerical minimization of  $\partial\Omega_3$  with respect to  $s$  at fixed  $\Omega_3$  then gives us

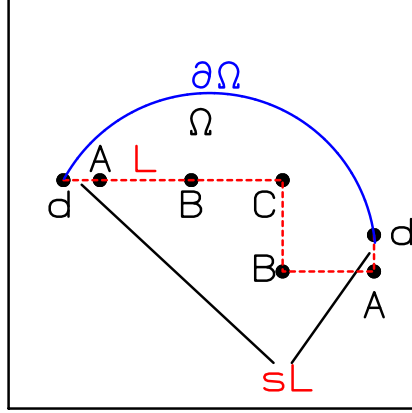


Figure 7: Generic droplet shape on SH lattice for a three corner droplet.

the equilibrium shape with three corners inside. Equating  $\partial\Omega_2 = \partial\Omega_3$  and  $\partial\Omega_3 = \partial\Omega_4 = 4L$  we find the volumes  $\Omega_{2/3}$  and  $\Omega_{3/4}$ , where the transitions to a three corner droplet occur. The actual transition values  $m_{1/2}, m_{2/3}$  and  $m_{3/4}$  are

$$\frac{m_{1/2}}{m_0} = \frac{2}{3}, \quad \frac{m_{2/3}}{m_0} = \frac{1}{3}, \quad \frac{m_{3/4}}{m_0} = 0.30237\dots, \quad (3.9)$$

where magnetization densities are given in units of the Onsager value  $m_0$ . In Fig. 8 we display the length of classical droplet surfaces as a function of  $\Omega/V$  for one, two, three and four corner droplets and transition points are marked by vertical lines. To determine the energy barriers at the  $2/3$  and  $3/4$  transitions we again argue, that for the saddle point configurations one needs to deform the 3 corner generic droplet shape of Fig. 7 for fixed volume at coexistence in such a way, that either point  $d$  of the figure collapses onto point  $A$ , or that an additional fourth corner is included. Both of these shapes are contained in (3.8) with  $s = 0$  for the volume  $\Omega_{2/3}$

and  $s = 1$  for  $\Omega_{3/4}$ . Using these we find for the excess lengths

$$\frac{\partial\Omega_{2/3} - \partial\Omega_2}{4L} = 0.02977... \quad (3.10)$$

$$\frac{\partial\Omega_{3/4} - \partial\Omega_3}{4L} = 0.03441... \quad (3.11)$$

with the largest barrier (3.11) being in fair agreement with the value (2.4) measured in the simulation.

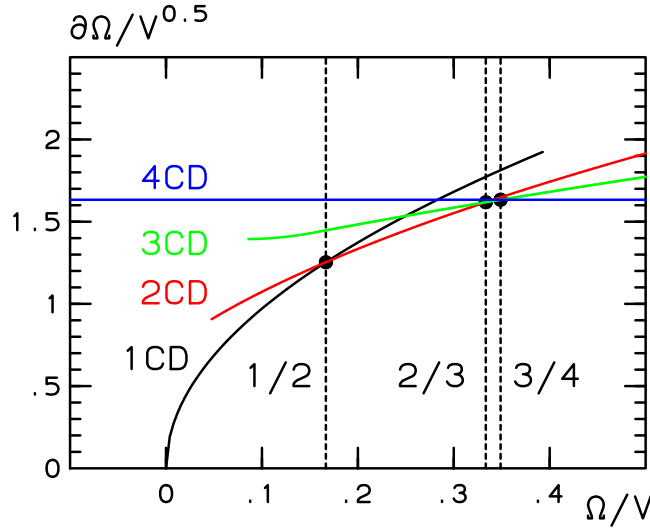


Figure 8: Classical droplet surfaces  $\partial\Omega/V^{0.5}$  on a SH lattice. The curves correspond to one, two, three and four corner droplets with vertical lines denoting the shape transition points.

#### 4. FINITE SIZE CORRECTIONS

In the limit of large box volumes  $V$  and large droplets the overall magnetization  $M$  in the two phase region is created by two areas with the Onsager value  $m_0$  for the magnetization density and opposite sign:  $M = (V - \Omega)m_0 - m_0\Omega$  and the droplet volume is a linear function of the overall density

$$\frac{\Omega}{V} = \frac{1}{2} \left( 1 - \frac{m}{m_0} \right). \quad (4.1)$$

There exists a variety of finite size effects, which all contribute to the droplet free energy and potentially modify relation (4.1) for the volume

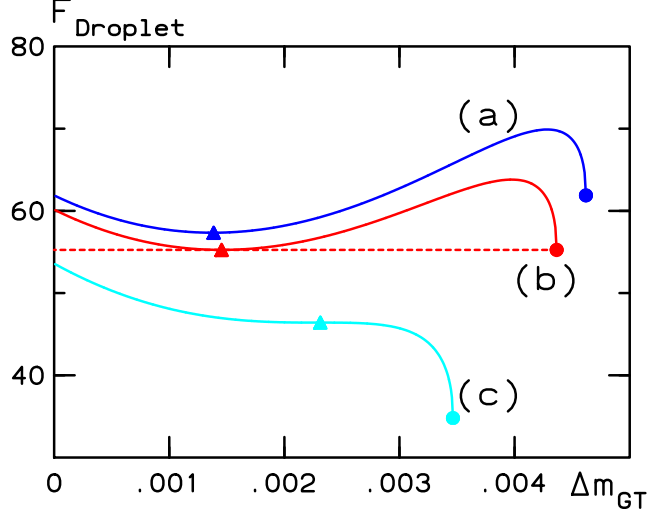


Figure 9: Droplet free energy  $F_{droplet}$  of (4.4) for three  $m$  values in vicinity and below  $m_0$  as a function of the Gibbs-Thomson shift  $\Delta m_{GT}$  with  $0 \leq \Delta m_{GT} \leq m_0 - m$ . With increasing values of  $m$  curves move from above to below. The saddle points of the droplet free energy are denoted by solid triangles, states with vanishing droplet volume correspond to solid circles. Curve (b) has a  $m$ -value right at the condensation phase transition point.

of the largest minority droplet on finite boxes. Corrections are due to the finite curvature of the droplet surface or due to the restrictions posed on fluctuations by the finite size of the droplet or the box, or by the presence of several droplets. The literature hosts the following corrections to a single droplet <sup>(17)</sup>

- Capillary wave corrections of surface string excitations with string length  $L$  contribute  $\ln(L)$  and constant terms to the free energy <sup>(26,27)</sup>, with presumably different coefficients in the strip and droplet state.
- Contributions to the free energy due to degeneracies of strip and droplet states under translations of the lattice cubic group. On a finite 2D system with pbc. a strip has a degeneracy  $2L$  and a droplet  $L^2$ . These entropic terms yield a contribution of order  $\ln(L)$  to the free energy. We expect this type of finite size effect to be present only at very low temperatures since the degeneracy is removed by

thermal excitations.

- Tolman corrections to the interface tension due to the small radius of curvature of very minute droplets <sup>(28,29,30)</sup>.
- Gibbs-Thomson corrections <sup>(31)</sup> describing a shift of the bulk magnetization due to the presence of curved surfaces.

It is very instructive also, to think of  $\Omega$  of (4.1) as an order parameter for the formation of an minority droplet of extensive size, which is non-zero in the two phase region and vanishes for all states with  $m > |m_0|$ . There exists actually then a phase transition associated with this order parameter, at which point the droplet either evaporates into a gas of “small” droplets, or the gas condenses. Again for infinite systems the phase transition is located exactly at the Onsager  $m_0$  value, but for finite systems corrections are present. Since all the above mentioned finite size effects may conspire in the observed shift of the transition it is an interesting and unsettled issue to study their contributions quantitatively. The droplet condensation phase transition has recently been studied with Monte-Carlo simulations of Ising-models with fixed magnetization in two <sup>(32)</sup> and three <sup>(33)</sup> dimensions. In these studies the size of the largest minority cluster was measured as a function of temperature i.e., along paths perpendicular to those we use, measuring at fixed temperature for various values of the magnetization. In  $d = 2$  the authors observed a discontinuous condensation phase transition with finite size effects similar to those of Fig. 17 and attributed them to the Gibbs-Thomson effect. We will quantify this statement with the following calculations and with the fits of section 5.3. In three dimensions the finite size analysis for the size of the largest minority cluster close to the transition is complicated by the fact, that for small enough magnetization there is a infinite percolating minority cluster present already in the one phase region <sup>(34)</sup>. The precise influence of this fact at the condensation transition deserves further investigation.

For the description of the condensation phase transition we assume that the finite box restricted  $m$  partition function of a possibly discontinuous transition can be written as

$$Z(m, L) = e^{-F_{droplet}(m,L)} + e^{-F_{bulk}(m,L)} \quad , \quad (4.2)$$

up to corrections exponentially small in  $L$  <sup>(35)</sup>, with  $F_{bulk}$  and  $F_{droplet}$  being suitable free energies in the one phase (bulk) and the two phase (droplet) region respectively. In the two phase region we use the classical theory for a single extensive droplet, as outlined in the preceding section, amended by Gibbs-Thomson (GT) corrections. The bulk phases are described by

Ginzburg Landau (GL) theory. The Gibbs-Thomson effect <sup>(31)</sup> accounts for a finite curvature of the surface of the droplet. Microscopically one can explain this effect by noting, that the average coordination number of a spin at a surface with positive curvature is reduced and thereby the rate of detachment into the phase of opposite sign is enhanced and the other way round for negative curvature. To lowest order this induces a small shift  $\Delta m_{GT}$  of the magnetization density of equal absolute value in both phases, but of opposite sign. Conservation of overall magnetization then leads to a shifted droplet volume

$$\frac{\Omega}{V} = \frac{1}{2} \left( 1 - \frac{m}{m_0} - \frac{\Delta m_{GT}}{m_0} \right) . \quad (4.3)$$

To calculate  $\Delta m_{GT}$  to lowest order we minimize the two phase free energy

$$F_{droplet} = \sigma \sqrt{4\pi\Omega} + c_2 V \Delta m_{GT}^2 , \quad (4.4)$$

where the first part is the surface free energy of a circular droplet of volume (size)  $\Omega$ , and the second part is the excess bulk free energy due to the shift  $\Delta m_{GT}$  in an expansion of the Ginzburg-Landau free energy up to second order around the bulk value  $F(\pm m_0)$ , which we choose to be zero for convenience. The coefficient  $c_2 = 18.1252318487\dots$  at  $\beta = 0.7$  is obtained from the low temperature series expansion results of <sup>(36)</sup>. Minimization of (4.4) results into  $\Delta m_{GT} \propto \partial\Omega^{-1}$  i.e., a shift of  $\Delta m_{GT}$  proportional to the curvature of the droplet, which after reinsertion into the free energy leads to a curvature dependent downward correction to the free energy. The droplet free energy (4.4) is displayed in Fig. 9 for three different values of  $m$  below  $m_0$  in close vicinity of  $m_0$  as a function of the Gibbs-Thomson shift  $\Delta m_{GT}$ , which for each  $m$  value in the figure ranges in-between  $\Delta m_{GT} = 0$  and  $\Delta m_{GT} = m_0 - m$ . With decreasing distance to Onsagers  $m_0$  the stable saddle point solution of situation (a) - as depicted in the figure - turns into a metastable one (b), which then turns unstable in situation (c), very close to  $m_0$ .

In finite systems the otherwise stable classical minority droplet of the two phase region becomes metastable at the condensation phase transition point  $m_{cond}(L)$ , where the system performs a finite size rounded transition into the one phase region. The condensation point shift due to the finite system size

$$\Delta m_{cond}(L) = m_0 - m_{cond}(L) , \quad (4.5)$$

corresponds to situation (b) as depicted in Fig. 9 and can be calculated by equating the free energy

$$F_{bulk} = V c_2 \Delta m_{cond}^2 \quad (4.6)$$



of the bulk state - the solid circles in Fig. 9 - to the saddle point free energy (4.4) in the two phase region: the solid triangles in Fig. 9. Note that the surface term in (4.4) depends also on  $\Delta m_{cond}$ . One finds the finite system condensation phase transition point

$$\Delta m_{cond}(L) = A_{cond} L^{-2/3} \quad (4.7)$$

on toroidal  $L^2$  boxes. The exponent  $-2/3$  for the finite-size behavior of the condensation transition was already found before in the context of metastable decay <sup>(1,6)</sup>, but the inclusion of Gibbs Thomson corrections lead to a different value of  $A_{cond}$ . The coefficient  $A_{cond}$  at  $\beta = 0.7$  has the value

$$A_{cond} = m_0 \eta \frac{3}{16^{1/3}} = 0.23697... \quad , \quad (4.8)$$

where parameter values  $\eta$  and  $\sigma$  are given by

$$\eta = \left[ \frac{\pi \sigma^2}{c_2^2 m_0^4} \right]^{1/3} = 0.20102... \quad (4.9)$$

$$\sigma = \sqrt{W/\pi} = 0.90358... \quad . \quad (4.10)$$

The droplet size  $\Omega_{cxc}(L)$  at the condensation phase transition is

$$\Omega_{cxc}(L) = \frac{V}{3} \frac{\Delta m_{cond}(L)}{m_0} = 0.07977... L^{4/3} \quad , \quad (4.11)$$

and one can also calculate the nucleation barrier  $B_{nucl}$ , which at the condensation phase transition corresponds to the maximal excess droplet free energy in-between states at the saddle point and states at  $\Delta m_{GT} = m_0 - m$ . One finds

$$\frac{B_{nucl}}{\sigma \sqrt{4\pi \Omega_{cxc}}} = 0.174038... \quad (4.12)$$

in units of the coexisting droplets surface free energy and  $B_{nucl}/F_{droplet} = 0.154701$  in units of the total free energy of the coexisting droplet. The Gibbs-Thomson corrected droplet loses its stability at the point

$$\Delta m_{unstable}(L) = m_0 \eta 6^{1/3} \left( \frac{3}{8} \right)^{2/3} L^{-2/3} \quad (4.13)$$

$$= 0.18808... L^{-2/3} \quad , \quad (4.14)$$

which inside of the metastable region terminates the droplet metastable branch. Condensation phase transition point scaling with the power law  $L^{-2/3}$  can also be proven with rigorous methods (see <sup>(37)</sup> for a recent

overview). Furthermore one finds at the condensation phase transition point the linear relation

$$\Delta m_{GT}(L) = \frac{1}{3} \Delta m_{cond}(L) \quad , \quad (4.15)$$

which expresses the Gibbs-Thomson shift in units of the finite size location of the phase transition point. This linear relation is especially interesting as the ratio

$$Q = \frac{V \Delta m_{cond}(L) / 2m_0}{\Omega_{cxc}(L)} \quad (4.16)$$

is predicted to have the value  $Q = 3/2$ . If one neglects Gibbs-Thomson corrections altogether one finds  $Q = 1$ . The value of  $Q$  does not depend on the particular values for the surface free energy, nor on the parameter value  $c_2$  (which all factor out in the calculation). A stringent test on the presence of Gibbs-Thomson corrections thus can be devised, if in the Monte-Carlo simulation one measures both, the coexisting droplets size  $\Omega_{cxc}(L)$  and location of the condensation phase transition  $\Delta m_{cond}(L)$ .

## 5. SIMULATION RESULTS

We have simulated the 2D Ising-model at  $\beta = 0.7$  ( $k_B T = 1.428 \dots$ ) on toroidal lattices and on cube-surface  $SH(L)$  lattices. In one set of Muca simulations we cover all states from the strip to the bulk phase and study  $L = 12$  up to  $L = 44$  toroidal  $L^2$  boxes and cube-surface lattices of parameter values  $L = 4$  up to  $L = 26$ . In another set of simulations the condensation point phase transition is studied on toroidal lattices of sizes  $40^2$  up to  $400^2$ , again also with the use of Muca simulations covering however a smaller  $m$ -interval in vicinity of the condensation phase transition.

### 5.1. SHAPE TRANSITIONS

In order to study the droplet shape transitions on the torus and on SH lattices in detail we consider the constraint magnetization ensemble of the Ising-model. Its partition function  $Z(m, L)$  is

$$Z(m, L) = \sum_{conf.} e^{-\beta H} \delta(m - \frac{1}{V} \sum_i s_i) \quad (5.1)$$

and we determine the expectation values of observables at fixed magnetization  $m$ . Muca ensemble simulations are perfectly suited for the evaluation of restricted expectation values. All one has to do is to average

over operator values at  $m$ , if the magnetization  $m$  is visited in the Muca simulation. As we are dealing with droplets it is sensible to introduce the  $m$ -dependent functions

$$\partial\Omega_0(m) = \sqrt{2\pi V(1 - \frac{m}{m_0})} \quad (5.2)$$

$$\Omega_0(m) = \frac{V}{2}(1 - \frac{m}{m_0}) \quad , \quad (5.3)$$

which for large system volume  $V$  denote the classical surface and volume of a circular droplet at fixed overall magnetization  $m$ . For each configuration at  $m$  we evaluate connectivity components i.e., clusters of spins. Nearest neighbor spins belong to the same cluster, if they have the same value. The size  $\Omega$  - the number of sites - is determined for each cluster and clusters are sorted with respect to their size. The second largest cluster defines the object of interest and corresponds to the minority phase droplet. Its expectation value in the magnetization bin  $m$  is denoted  $\langle \Omega \rangle (m)$ , the “volume” of the minority phase droplet. It should be noted that  $\langle \Omega \rangle (m)$  not necessarily has to agree with  $\Omega_0(m)$ , if finite size effects are present. For the toroidal lattice geometry (pbc.) and for the minority phase droplet a rectangular bounding box with linear sizes  $L_1$  and  $L_2$  is determined in such a way, that the droplet exactly fits into the box. From the geometric numbers  $L_1$  and  $L_2$  two geometric order parameters are formed, namely

$$O_1(m) = \delta(L - \max(L_1, L_2)) \quad (5.4)$$

$$O_2(m) = \frac{\max(L_1, L_2)}{L} \quad . \quad (5.5)$$

Values for the operator  $O_1(m)$  are zero and unity. At the position  $m_{D/S}$  of the droplet strip transition we expect to find a finite size rounded jump of the expectation value  $\langle O_1(m) \rangle$  from value zero to unity. The order parameter  $O_2(m)$  on the other hand has several discrete values in the interval  $[0, 1]$ . One can construct a probability distribution function  $P(O_2)$  for the occurrence of values  $O_2$  in the restricted partition function (5.1) at  $m$ . If our classical arguments on the nature of the droplet to strip transition are correct, then one expects to find a double peaked distribution function  $P(O_2)$  in the vicinity of  $m_{D/S}$  with a barrier, which is related to the excess length. Susceptibilities  $C_1(m)$  and  $C_2(m)$  are defined by

$$C_1(m) = L \langle (O_1(m) - \langle O_1(m) \rangle)^2 \rangle \quad (5.6)$$

and similar for  $C_2(m)$  with  $O_2$ , where  $\langle \rangle$  again denotes the expectation value at given  $m$ . These susceptibilities show a finite size rounded peak at the shape transition defining finite size shifted  $m_{D/S}(L)$ -values.

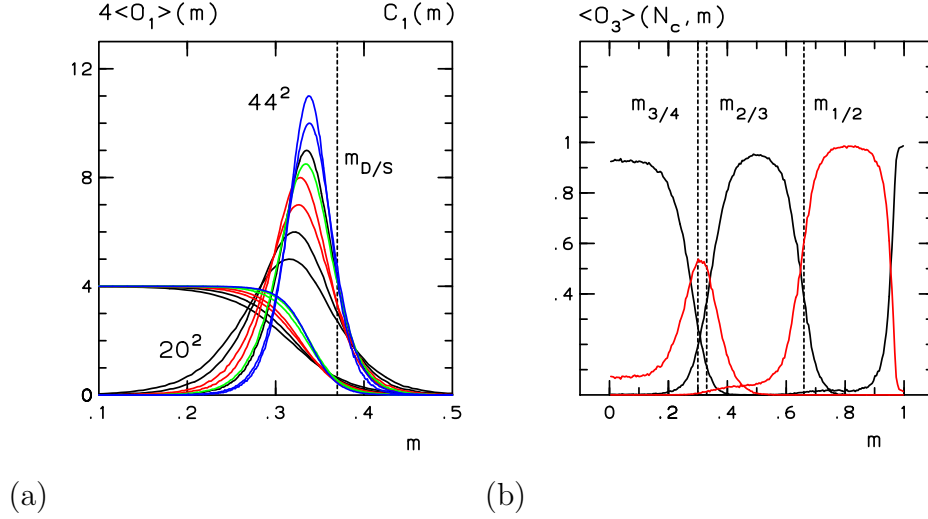


Figure 10: (a): Droplet to strip transition geometric order parameter  $4\langle O_1(m) \rangle$  and susceptibility  $C_1(m)$  for the torus with pbc. and (b): geometric order parameter  $\langle O_3(m, N_c) \rangle$  on a  $SH(26)$  lattice with  $N_c = 0, 1, 2, 3$  and  $N_c = 4$ . The 5 different  $N_c$ -dependent curves have maxima, which from the right to the left correspond to values  $N_c = 0, 1, 2, 3$  and to  $N_c = 4$ . Vertical lines denote classical shape transition points.

For the minority droplet on SH lattices we define a geometric order parameter sensitive to the number  $n_c$  of corners occupied by the droplet. At magnetization  $m$  we count the number  $n_c$  and define

$$O_3(m, N_c) = \delta(N_c - n_c) \quad , \quad (5.7)$$

which at given  $m$  receives unity contributions only if  $N_c$  corners are occupied. We expect e.g., that expectation values  $\langle O_3(m, 2) \rangle$  yield non-vanishing values  $\langle O_3(m, 2) \rangle \approx 1$  only, if the magnetization density  $m$  lies in-between the  $1/2$  and  $2/3$  shape transition magnetization density values. Data for the geometric order parameters  $\langle O_1 \rangle(m)$  on toroidal lattices and data for  $\langle O_3(m, N_c) \rangle$  with  $N_c = 0, \dots, 4$  on a  $SH(26)$  lattice are displayed in Figs. 10a and 10b. The maximum positions of the susceptibility in Fig. 10a on toroidal lattices define finite volume estimates of the magnetization density  $m_{D/S}$  at coexistence. Finite size correction are not particularly small and thus a careful infinite volume extrapolation is needed. For every pair of values  $L$  and  $m_{D/S}(L)$  we calculate

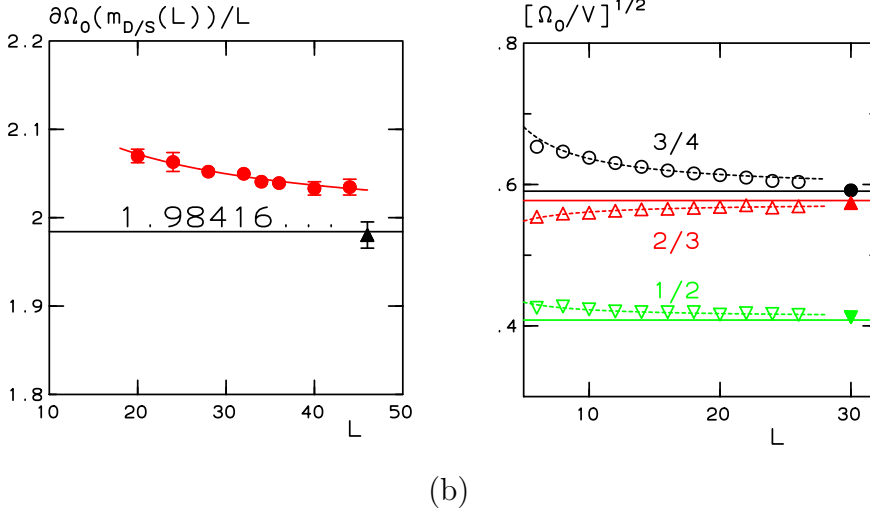


Figure 11: (a): Fit to  $m_{D/S}$  on the torus. The function  $\partial\Omega_0/L$  is evaluated at the measured finite size shifted values of  $m_{D/S}(L)$  and plotted as a function of  $L$ . The line corresponds to the exact result, while the solid triangle corresponds to the infinite volume extrapolation. The curve corresponds to the fit as explained in the text. (b): Fit to the three shape transition points on  $SH(L)$  lattices. Here the function  $\sqrt{\Omega_0/V}$  is evaluated at the measured finite size shifted magnetization density values and plotted as a function of  $L$ . Again horizontal lines correspond to droplet calculations, while curves correspond to fits explained in the text. Solid symbols correspond to the infinite volume extrapolation.

$\partial\Omega_0(m_{D/S}(L))/L$  and with the use of the extrapolation

$$\partial\Omega_0(m_{D/S}(L))/L = \sqrt{2\pi(1 - \frac{m_{D/S}}{m_0})} + A_{D/S} \frac{\ln(L)}{L} \quad (5.8)$$

$m_{D/S}$  is determined. We mention, that  $\ln(L)/L$  finite size corrections are predicted by capillary wave fluctuation corrections to the droplet free energy<sup>(26,27)</sup> and by entropic terms. The fit in accord with (5.8) has a  $\chi^2_{dof}$  value 0.32 and results into a transition point at  $m_{D/S} = 0.376(9)$ , which within error bars coincides with the exact result (3.3). The data and the fit are displayed in Fig. 11a. A similar analysis based on  $C_2(m)$  data yields the determination  $m_{D/S} = 0.360(10)$ , which again agrees with the exact result. Similar as in torus case we also calculate susceptibilities of the  $O_3$  order parameter on  $SH(L)$  lattices and determine finite size shifted shape transition points. The results are displayed in Fig. 11b as

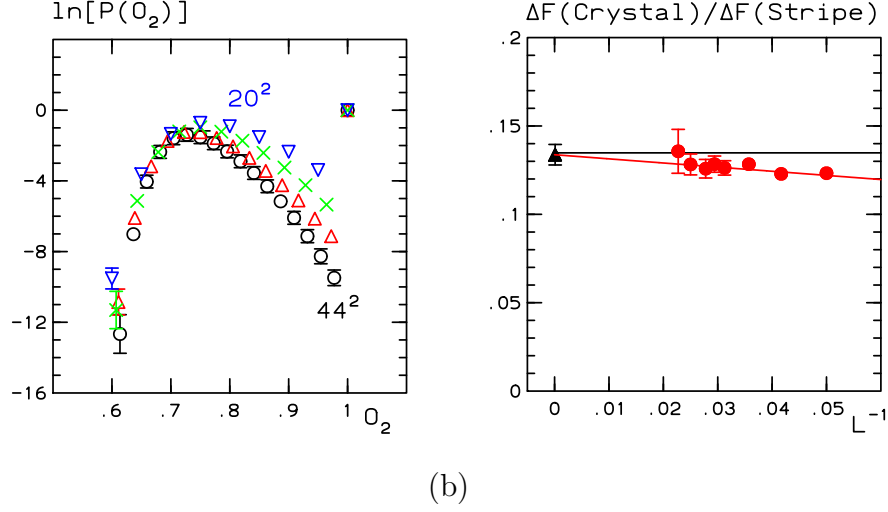


Figure 12: (a) Geometric order parameter  $O_2$  distribution on the torus in vicinity of  $m_{D/S}$  and (b) barrier values as a function of  $1/L$ . The horizontal line denotes the classical droplet theory result, the solid triangle the infinite volume extrapolation.

a function of  $L$  on  $SH(L)$  lattices. In this case three different  $i = 1, 2, 3$  infinite volume transition points are determined via the extrapolation

$$\sqrt{\frac{\Omega_0(m_{i/i+1}(L))}{V}} = \sqrt{\frac{1}{2}\left(1 - \frac{m_{i/i+1}}{m_0}\right)} + B_{i/i+1} \frac{1}{L} \quad . \quad (5.9)$$

We did not include a  $\ln(L)/L$  term in this Ansatz, since capillary wave corrections are the same on both sides of the transition and entropic terms should be absent since the droplets center of mass is energetically pinned. We obtain the values  $m_{1/2} = 0.661(2) m_0$ ,  $m_{2/3} = 0.342(3) m_0$  and  $m_{3/4} = 0.305(3) m_0$ , which within a systematic one percent relative error all agree with the values of (3.9). The small discrepancy is presumably caused by the isotropic surface free energy of our (approximative) droplet calculation for  $SH$  lattices. The susceptibility  $C_2(m)$  on toroidal lattices has its maximum value at positions  $m_{D/S}(L)$  and we can determine the probability distribution  $P(O_2)$  of the order parameter  $O_2$  there. The data are displayed in Fig. 12a for  $L = 20, 28, 36$  and  $L = 44$  lattices. One observes clear double peaks with the peak for the strip concentrated in the single point at  $O_2 = 1$ . In-between one finds states, which with increasing lattice size become less and less probable. These suppressed states are the saddle point crystal shapes of Fig. 4. A split of phase space

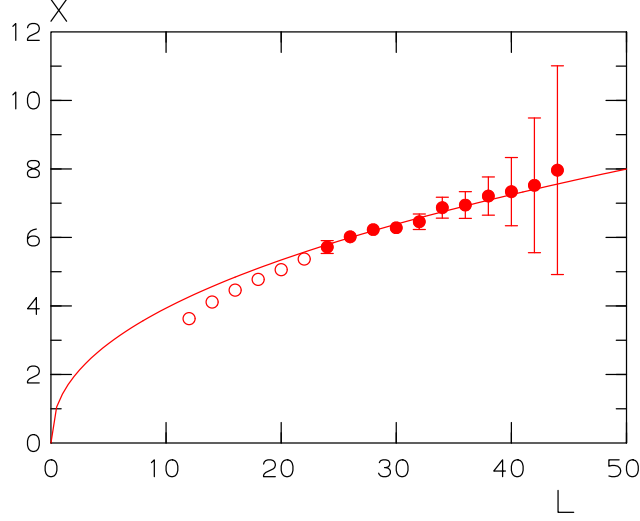


Figure 13:  $X$  values as defined in (5.13) as a function of  $L$  and fit as explained in the text.

into two disconnected regions with a free energy barrier in-between proves the discontinuous nature of the droplet strip transition and one can determine the barrier height. The distribution functions have two maxima values  $P_{max,1}$  and  $P_{max,2}$  and a minimum value  $P_{min}$ . We form

$$\Delta F_{droplet} = \frac{1}{2} \ln(P_{max,1} P_{max,2} / P_{min}^2) \quad , \quad (5.10)$$

which we measure in units of  $\Delta F_{strip} = 2L\sigma_0$  and the result is displayed in Fig. 12b as a function of  $1/L$ . A linear fit in  $L^{-1}$  (the curve in the figure) results into the value

$$\Delta F_{droplet} / \Delta F_{strip} = 0.133(6) \quad (5.11)$$

at a  $\chi^2_{dof}$  value 0.40 for the fit. The free energy barrier measured in exponential slowing down of Muca simulation (2.3) agrees with the free energy barrier measured in the suppression of saddle point crystal shapes (5.11) and with the result of classical droplet theory (3.4).

## 5.2. MORE DROPLET FREE ENERGY CORRECTIONS

A direct consequence of a discontinuous behavior of the restricted partition function  $Z(m, L)$  at the droplet strip shape transition  $m_{D/S}$  on

the torus is again the validity of a superposition Ansatz <sup>(35)</sup>

$$Z(m, L) = e^{-F_{strip}(m, L)} + e^{-F_{droplet}(m, L)} \quad , \quad (5.12)$$

which we use to determine free energy corrections. If we define the quantity

$$X = \frac{Z(m = m_{D/S}, L)}{Z(m = 0, L)} - 1 \quad (5.13)$$

we observe, that classical bulk and surface free energy contributions proportional to  $L^2$  and  $L$  cancel in  $F_{strip}(m = 0, L) - F_{droplet}(m = m_{D/S}, L)$ . Note that the classical surface contributions to the free energy of a strip state at  $m = 0$  equal those at  $m = m_{D/S}$  and in addition classical surface portions of  $F_{strip}$  equal those of  $F_{droplet}$  at  $m = m_{D/S}$ . We obtain the representation

$$X = e^{G_{strip}(m=0, L) - G_{droplet}(m=m_{D/S}, L)} \quad (5.14)$$

where the  $L$ -dependence of the function  $G$  at most is of the order  $o(L)$  and possibly contains the whole set of finite size corrections to strip and droplet states.

One of the quantities, which in the Muca simulation is determined, is the magnetization probability  $P_L(M)$ . It counts the probability to find magnetization  $M$  in the unconstrained Ising model and is proportional to the constraint partition function  $P_L(M = mV) \propto Z(m, L)$ . The value  $P_L(M = 0)$  is easily measured at the magnetization bin  $M = 0$ , while  $Z(m = m_{D/S}, L)$  with  $m_{D/S} = 0.36974\dots$  is interpolated from data at magnetization bins closest to the value  $Vm_{D/S}$ . Fig. 13 displays the data for  $X$  as a function of  $L$ . Right at the crystal shape transition and with increasing lattice size droplet states relative to strips turn out to be more and more probable. For large systems the data can be fitted with a power law in  $L$  (the solid symbols in the figure)

$$X = A_X L^\alpha \quad (5.15)$$

and at a  $\chi_{dof}^2$  value of 0.12 we obtain with  $A_X = 1.4(4)$  an exponent value of  $\alpha = 0.44(8)$ . Such finite size effects do not have their origin in Gibbs-Thomson corrections but either are generated by capillary wave fluctuation corrections - or by the count of strip and droplet states with respect to translations. At zero temperature each translational degree of freedom reduces the free energy by a term  $-\ln(L)$  and for finite temperature, each fluctuating surface contributes  $+\frac{1}{2}\ln(L)$  via the capillary wave expansion. Our theoretical prediction for  $\alpha$  therefore is  $\alpha = -1 + 2(\frac{1}{2}) + 2 - \frac{1}{2} = 3/2$ ,



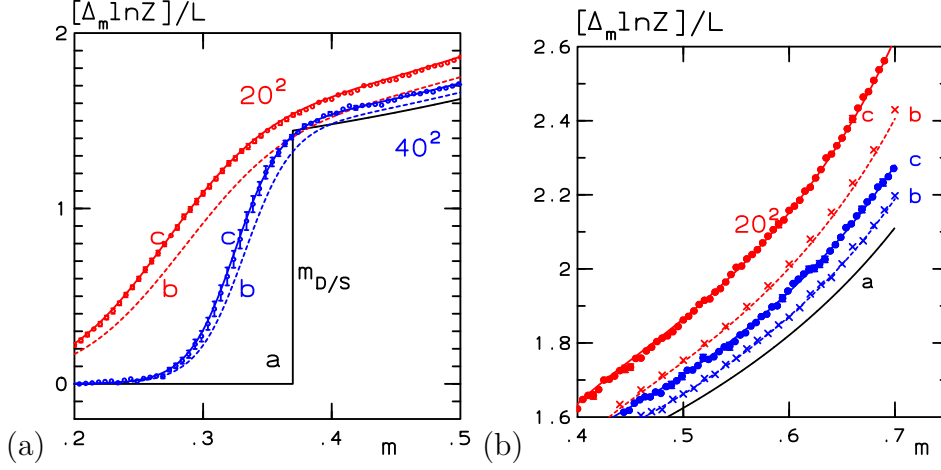


Figure 14: Finite size rounding of the discrete derivative  $(\Delta_m \ln Z)/L$  in vicinity of the crystal shape transition (a) and in the droplet phase (b). For reasons of clarity we only present data for two lattice sizes,  $20^2$  and  $40^2$ . The curves labeled “c” in the figures exactly match the measured data (circles) and correspond to theoretical predictions for droplet and strip free energies. The data denoted by crosses in (b) are results from a simulation with a modified partition function (one spin is fixed to  $-1$ ) and agree with curves labeled “b”. These are based on the droplet free energy without logarithmic phase space factor in the droplet volume.

if translational degeneracies are counted - or  $\alpha = 2(\frac{1}{2}) - \frac{1}{2} = 1/2$ , if temperature lifts degeneracies. The measured value is consistent with one half and thus temperature is too high for a “naive” zero temperature count of degeneracies. Note, that two independent surface strings were assumed for the strip and one for the droplet. To probe free energies further, we introduce the discrete  $m$  partition function derivative

$$\Delta_m \ln Z := \frac{\ln Z(m + \Delta_M/V, L) - \ln Z(m, L)}{(\Delta_M/V)}, \quad (5.16)$$

which for small  $\Delta_M$  is proportional to  $\frac{\partial F(m)}{\partial m}|_{T,V}$ . Thus  $\Delta_m \ln Z/L^d$  can be interpreted as a magnetic field <sup>(9)</sup> or as a chemical potential <sup>(8)</sup> in the lattice gas interpretation. We have chosen a suitable value  $\Delta_M = 20$  and the measured Monte Carlo data are displayed in Figs. 14a and 14b for  $m$ -values in vicinity of  $m = m_{D/S}$  in (a) and for  $m$  values in the droplet phase in (b). Similar data for the 2D Ising model at temperature  $T = 0.8T_c$ , presented in Fig. 10 of <sup>(9)</sup>, also showed the presence of the strongly rounded stripe droplet transition, without attempting a quantitative fit of the data. For reasons of clarity we only present results for two lattices,  $20^2$  and  $40^2$

in size. The data, the circles in the figures, can be compared to several finite size rounding predictions (the curves in the figures), which are based on the superposition Ansatz (5.12). The infinite volume prediction, which is labeled “a”, jumps at  $m_{D/S}$  from the value zero (strip phase) to a finite value (gap) and in the droplet phase follows the classical result (3.1). The curves labeled “b” in the figure correspond to finite size rounding in accord with (5.12) and with free energy functions

$$F_{strip} = 2\sigma_0 L + \ln(L) \quad (5.17)$$

$$F_{droplet} = \sigma\sqrt{4\pi\Omega} + c_2 V \Delta m_{GT}^2 + \frac{1}{2} \ln(\partial\Omega) \quad (5.18)$$

including classical terms as well as capillary wave fluctuations corrections. As can be noted, the presence of further correction terms is suggested.

The translational invariance of a droplet of  $-$  spins floating in a background of  $+$  spins can easily be broken, if one spin of the partition function  $Z_{droplet}$  is fixed to the value  $-1$ , which in consequence lowers the partition function by a factor  $f$ :  $Z_{fixed\ spin} = f Z_{droplet}$  with  $f < 1$ . At zero temperature one finds  $f = \Omega/V$  and thus a “microcanonical droplet phase space volume” correction to the droplet free energy of the form

$$\hat{F}_{droplet} = F_{droplet} + \ln\left(\frac{\Omega}{V}\right) \quad , \quad (5.19)$$

quite similar to the microcanonical phase space volume of gases, is predicted. Adding this term to the droplet free energy in the droplet phase moves curves labeled “b” to curves labeled “c” in Fig. 14b, which exactly reproduce the data. One can also do a simulation in the modified theory, which differs from the original one by the fixation of one arbitrary single spin to the value  $-1$ , which never is updated. The crosses of Fig. 14b correspond to data from such a simulation and as can be seen: they come to lie on the curves labeled “b”, the free energy form without logarithmic phase space factor in the droplet volume.

It is interesting to ask the non-trivial question, whether similar phase space corrections contribute to the strip free energy. Strips are separated from droplets by barriers and thus the full occupancy of phase space (with logarithmic phase space factor in the droplet volume) may never be reached. A situation like this can be termed: spontaneous breaking of translational invariance for strip states, which according to our findings actually is realized in the  $\beta = 0.7$  2D Ising model. The curves labeled (c) of Fig. 14a have been calculated with the droplet free energy  $\hat{F}_{droplet}$  and with

$$\hat{F}_{strip} = F_{strip} - \ln(2) \quad (5.20)$$

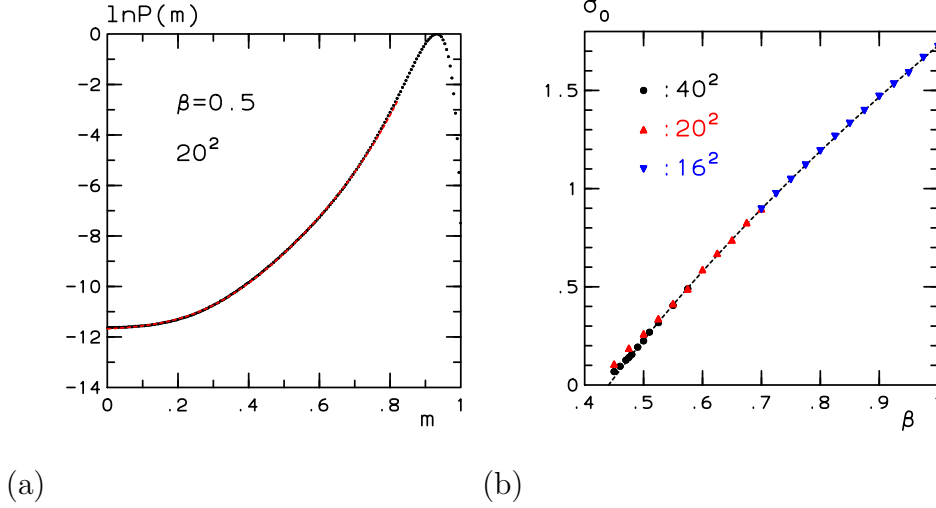


Figure 15: (a) Logarithmized magnetization density probability distribution data as a function of  $m$  at  $\beta = 0.5$  ( $T/T_c = 0.88$ ) on a  $20^2$  box and finite size rounding fit as explained in the text. Data and the fitted curve lie on top of each other. The fitted infinite volume interface tension  $\sigma_0$  is displayed in (b) as a function of  $\beta$ . The curve in (b) corresponds to the exact result.

and coincide exactly with the data. The strip free energy lacks logarithmic phase space factors, which are inconsistent with the measurement and we have included a constant correction term. Each droplet at the crystal phase transition tunnels into either one of two possible different strip configurations and thus the strip free energy is lowered by a term  $-\ln(2)$ .

Droplet and strip free energies of Eqs. (5.19) and (5.20) can be used to determine the interface tension  $\sigma_0$  from the finite size rounding of the free energy at the crystal shape transition. If for practical purposes we approximate the droplet free energy by

$$F_{\text{droplet}} \approx \sigma \partial \Omega_0(m) + \frac{\alpha_{GT}}{\partial \Omega_0(m)^2} + \ln\left(\frac{\Omega}{V}\right) \quad (5.21)$$

we obtain with Eq. (5.12) and with  $\ln Z(m, L) = \ln P_L(m) + \text{const}$  at fixed  $m_0$  a four parameter representation of the free energy as a function of the parameters  $\sigma_0, \sigma, \alpha_{GT}$  and  $\text{const}$ , which easily can be fitted. A typical set of data for the logarithmized free energy at  $\beta = 0.5$  on a  $20^2$  box is displayed in Fig. 15a and the fit for values  $m < 0.8m_0$  (droplet and strip phases) lies right on top of the data. Figure 15b displays the interface tension  $\sigma_0$  as determined from rather small boxes as a function of  $\beta$  in

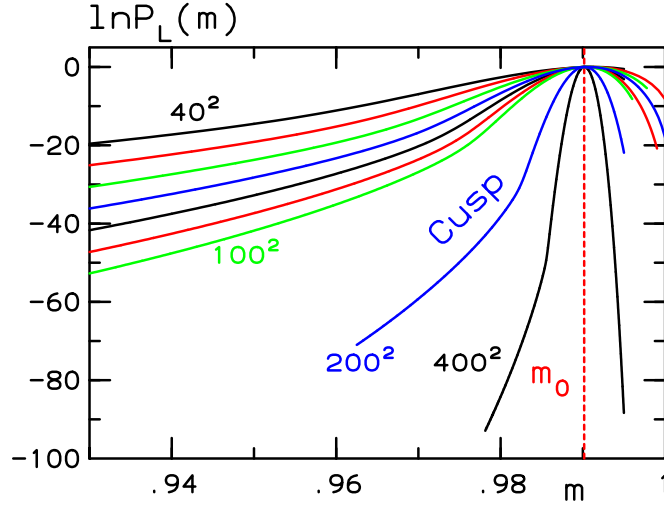


Figure 16: Logarithmized magnetization density probability distribution functions  $P_L(m)$  on toroidal  $L^2$  boxes at  $\beta = 0.7$  for the 2D Ising model. The maxima are normalized to values unity in  $P_L(m)$ . One observes almost Gaussian fluctuations in vicinity of  $m_0$ . Once one approaches the two phase separated phase space region, a finite size rounded cusp structure appears, which corresponds to the condensation phase transition.

comparison to the exact result, the curve in the figure. The agreement is excellent demonstrating, that finite size corrections of the free energy are faithfully represented.

### 5.3. CONDENSATION PHASE TRANSITION

The phase transition of an extensive minority droplet in the phase separated phase space region into a gas of small droplets in the bulk phase is studied on toroidal lattices. In order to provide an overview over the data we display in Fig. 16 the (logarithmized) probability distribution  $P_L(m)$  of the magnetization density - the constraint partition function  $Z(m, L)$  - as a function of  $m$  in vicinity of Onsagers magnetization density value  $m_0$ . A finite size rounded cusp structure is visible for values of  $m$  slightly below  $m_0$  and corresponds to the position of the condensation phase transition  $m_{cond}(L)$ . The data are obtained on  $40^2$  up to  $400^2$  boxes with the help of Muca simulations, which quite similar to simulations with the Wang-Landau algorithm (see section 2) also suffer from exponential

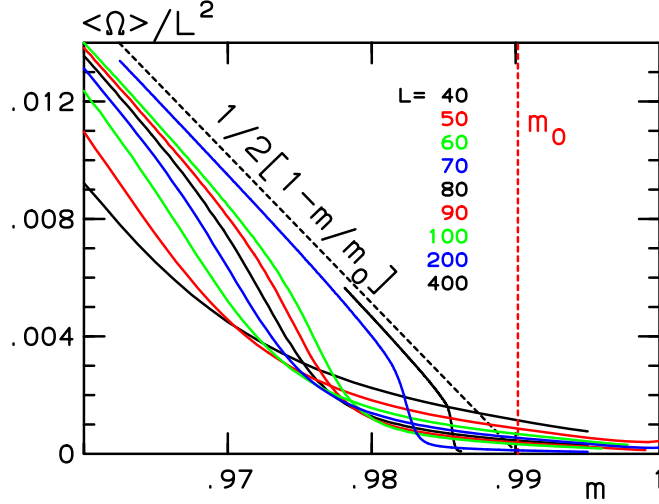


Figure 17: Expectation values  $\langle \Omega \rangle (m)/L^2$  for the minority droplet size density in vicinity of the condensation point phase transition for  $40^2$  up to  $400^2$  boxes. The infinite volume prediction  $(1 - m/m_0)/2$  corresponds to the dashed diagonal straight line.

down and in fact: it would be quite time consuming to obtain data of comparable statistical quality for a  $1000^2$  box.

The expectation value for the size of the minority droplet  $\langle \Omega \rangle (m)$  is displayed in Fig. 17. From the peak positions of the  $\Omega$  susceptibility (not displayed in a figure) we determine finite size shifted condensation point magnetization values  $m_{cond}(L)$  and calculate the shift due to the finite system size  $\Delta m_{cond}(L) = m_0 - m_{cond}(L)$ . The shift is displayed in Fig. 18 in a double logarithmic scale as a function of  $L$ . Numerical values are contained in table 1. The condensation point shift of Fig. 18 contains a straight line, which corresponds to the theoretical prediction of classical droplet theory with Gibbs-Thomson corrections (4.7). While finite size corrections to the theory on small boxes are large, it appears perfectly possible, that the data (the solid circles in the figure) approach the theoretical prediction on large boxes i.e., for large droplets. Additional finite size corrections are caused by sub-leading free energy contributions and quite similar to the discussion of section 5.2, we compare in Fig. 19 data for the discrete derivative  $\Delta_m \ln Z$  on  $200^2$  and  $400^2$  boxes with finite size rounding theory, as predicted by the superposition Ansatz (4.2). Simi-

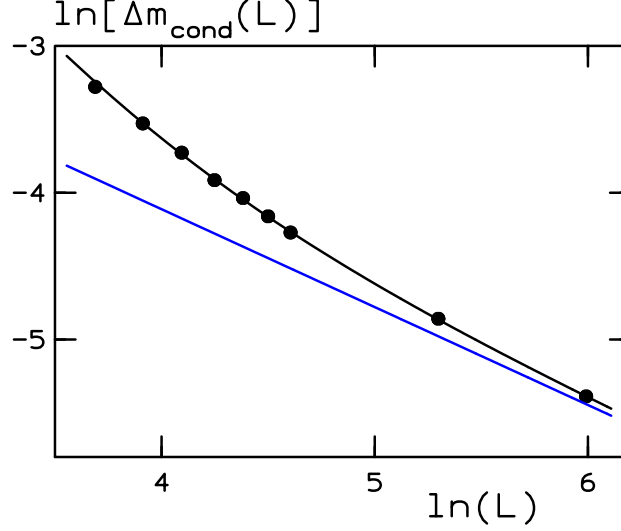


Figure 18: Condensation point phase transition transition points at  $\beta = 0.7$  in the 2D Ising model. The straight line corresponds to the theoretical prediction, including Gibbs-Thomson corrections. The curve corresponds to a fit to Eq. (5.24) as explained in the text.

lar Monte-Carlo data for systems of smaller linear extent were shown in Fig. 10 of <sup>(9)</sup> for the Ising model in  $D=2$  and in Figs. 6 and 7 of <sup>(8)</sup> for  $D=3$ . The onset of the same singularity as displayed in Fig. 19 is clearly visible in those data, despite of the presence of strong finite-size rounding. The Ansatz now uses the precisely known droplet free energy of (5.19) and the bulk free energy of (4.6). The dashed lines of the figure do correspond to finite size rounding predictions. It is evident, that the second order expansion of the Ginzburg-Landau free energy is not precise enough. The calculation of coefficients  $c_n$

$$U_{eff}(m) = \sum_{n=2}^{\infty} c_n (m - m_0)^n \quad (5.22)$$

of an polynomial expansion for the constraint effective potential  $U_{eff}(m)$

$$U_{eff}(m) = \lim_{L \rightarrow \infty} \left[ -\frac{1}{L^2} \ln Z(m, L) \right] \quad (5.23)$$

in higher powers of  $m - m_0$ , could provide a better bulk free energy form. We will not however pursue this issue here.

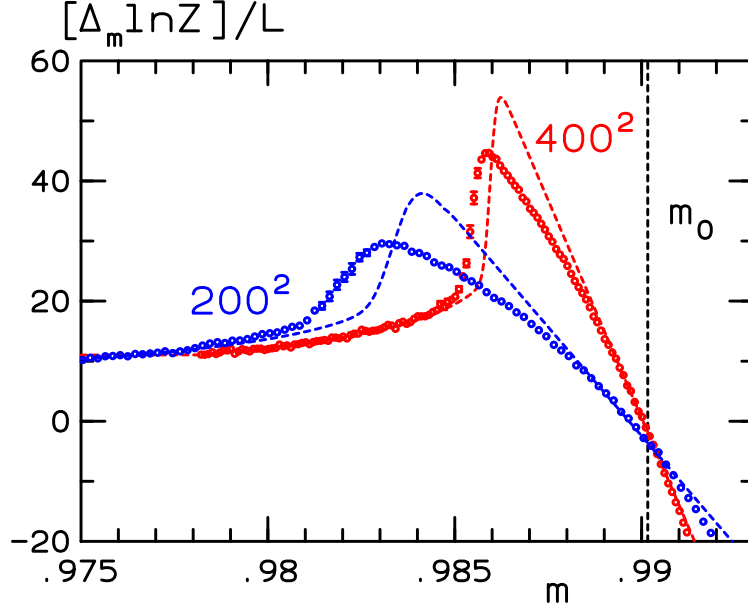


Figure 19: Finite size rounding of data for the discrete derivative  $(\Delta_m \ln Z)/L$  as defined in Eq. (5.16) for  $m$  values in vicinity of the condensation phase transition on two lattice sizes,  $200^2$  and  $400^2$ . The dashed curves correspond to finite size rounding predictions. Discrepancies are observed for bulk states slightly above the finite system phase transitions. The effect is due to the second order Ginzburg-Landau free energy expansion.

We perform a three parameter fit to  $\Delta m_{cond}(L)$  data and parameterize additional finite size corrections through a single power correction with a free exponent value  $\beta$

$$\Delta m_{cond}(L) = A_{cond} L^{-2/3} + B L^{-\beta} \quad . \quad (5.24)$$

The fit corresponds to the curve in Fig. 18 and at a  $\chi^2_{dof}$  value of 0.25 we obtain the fit parameters  $B = 23(9)$ ,  $\beta = 1.93(11)$  and  $A_{cond} = 0.237(3)$ . The fitted value for  $A_{cond}$  perfectly agrees with the theoretical prediction  $A_{cond} = 0.23697\dots$  (4.8), which at the condensation phase transition yields support for the validity of classical droplet theory and the presence of Gibbs-Thomson corrections for large droplets. A somewhat more stringent test of the presence of Gibbs-Thomson corrections can be devised, if at the condensation phase transition the ratio  $Q$  of (4.16) is calculated. For large droplets one expects, that  $Q$  equals  $Q = 3/2$ . For magnetization values at - or close to - the condensation transition, we determine the probability distribution  $P_L(\Omega)$  for the occurrence of a minority droplet

L	$\Delta m_{cond}$	$\Omega_{cxc}/L^{2/3}$	$\Omega_{cxc}$	$Q$	$B_{cxc}/\sigma\sqrt{4\pi\Omega_{cxc}}$
40	0.0376(12)	-	-	-	-
50	0.02936(80)	-	-	-	-
60	0.02405(55)	-	-	-	-
70	0.01995(40)	-	-	-	-
80	0.01766(31)	-	-	-	-
90	0.01559(24)	-	-	-	-
100	0.01396(20)	0.0976(8)	45.3(4)	1.555(25)	0.013(2)
200	0.007762(50)	0.0878(5)	102.7(6)	1.526(12)	0.045(4)
400	0.004575(12)	0.0825(9)	243.4(6)	1.518(16)	0.085(4)
$\infty$	0.	0.07977...	$\infty$	1.5	0.17404...

Table 1: Measured observables for the 2D Ising model droplet condensation phase transition at  $\beta = 0.7$ . The lowest line contains the infinite volume theoretical predictions of classical droplet theory with Gibbs-Thomson corrections.

of size  $\Omega$  in the magnetization constraint partition function at  $m$  and tune the magnetization values to the point, where finite system double peaked probability distributions have equal height. The result  $P_L(\Omega)$  is displayed in Fig. 20 as a function of  $\Omega/L^{4/3}$  for boxes  $100^2$ ,  $200^2$  and  $400^2$ .

Our numerical simulation demonstrates the existence of double peaks in  $P_L(\Omega)$ . There also exists a barrier for states in-between, which increases with increasing droplet size. These findings provide numerical evidence for the fact, that the droplet condensation phase transition of the 2D Ising model is of discontinuous nature. Upon fitting Gaussians to the right hand side peaks of Fig. 20 we determine values for the coexisting droplets size  $\Omega_{cxc}$ , which are contained in rows three and four of table 1. Values for the ratio  $Q$  are given in the fifth row of table 1. On the  $400^2$  box we find  $Q = 1.518(16)$ , which indeed is very close to  $Q = 3/2$  and thus again provides solid support for the asymptotic correctness of classical droplet theory and the presence of Gibbs-Thomson corrections.

A very interesting quantity is the nucleation barrier  $B_{nucl}$ , which at the condensation phase transition determines the suppression of states in-between the equilibrium minority droplet - and the gas of small droplets in the bulk phase. At equal height of the probability distribution  $B_{nucl}$  can be estimated through

$$B_{nucl} \approx \ln \frac{P_{max}}{P_{min}} \quad , \quad (5.25)$$

where values  $P_{max}$  and  $P_{min}$  denote maxima and minima of  $P_L(\Omega)$ . The last row of table 1 contains  $B_{nucl}$  values, which are given in units of the



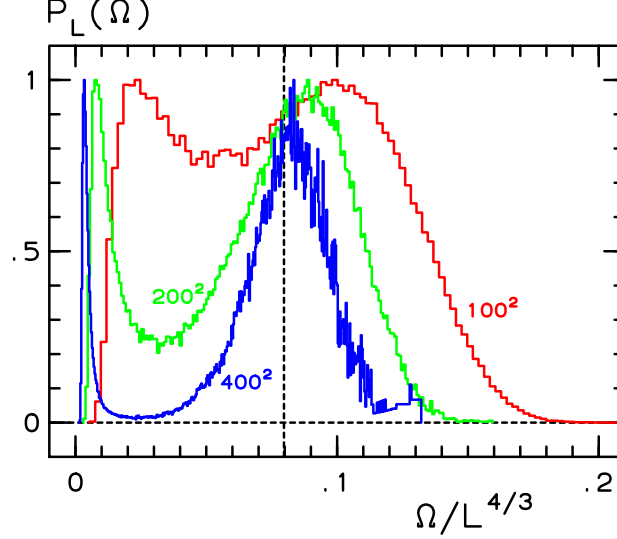


Figure 20: Probability distributions  $P_L(\Omega)$  of the minority droplet size at the condensation phase transition. The vertical line corresponds to the “gap” prediction of classical droplet theory with Gibbs-Thomson corrections.

droplet surface free energy  $\sigma\sqrt{4\pi\Omega_{cxc}}$ . The data exhibit large finite size effects and most likely one needs much larger droplets in order to draw definite conclusions. On the  $400^2$  box we find a barrier, which is smaller by a factor of  $1/2$  than the theoretical prediction (4.12). Chances thus are high, that the condensation of large droplets proceeds within Gibbs-Thomson corrected classical droplet theory through the formation of intermediate saddle point configurations, which are classical in nature also.

The grand-canonical droplet model of <sup>(18,19)</sup> predicts

$$\Omega_{crit} = \left[ \frac{(d-1)\hat{\sigma}}{2dm_0h} \right]^d \quad d \geq 2 \quad . \quad (5.26)$$

for the volume  $\Omega_{crit}$  of the instable critical droplet as a function of the ordering field  $h$ . Taking into account that the the surface tension  $\hat{\sigma} = \sqrt{4\pi}\sigma$  of <sup>(18,19)</sup> differs from ours by a factor  $\sqrt{4\pi}$  one obtains

$$\Omega_{crit} = \frac{\pi\sigma^2}{4m_0^2h^2} \quad (5.27)$$

in  $d = 2$ . Using Eq. (4.11) and  $\Delta m = h/2c_2$  we compare  $\Omega_{crit}$  with the

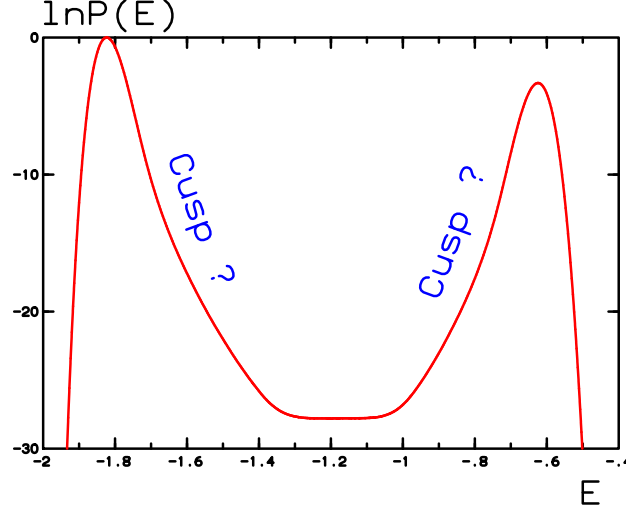


Figure 21: Probability distribution  $P(E)$  for the energy in the 2D  $q = 20$  Potts model on a  $70^2$  box. The conjectured positions of condensation phase transitions are indicated by finite size rounded cusps.

volume of the equilibrium droplet at the condensation phase transition

$$\Omega_{cxc} = \frac{A_{cond}^3}{3m_0\Delta m_{cond}^2} = 9 \frac{\pi\sigma^2}{4m_0^2 h_{cond}^2} \quad , \quad (5.28)$$

which has the same field dependence as (5.27).  $\Omega_{cxc}$  is a factor nine times larger than  $\Omega_{crit}$ . As one can see in Fig. 20 this is in accordance with our simulations. The droplet volume ratios of the stable droplet at coexistence over the critical droplet at the saddle point approximately have values 2, 3 and 4 for the considered lattice sizes. It is very well possible, that these volume ratios approach the predicted value 9 in the infinite volume limit.

Finally we want to discuss how the free energy  $F_L = \ln P_L(M)$  in general and the observed transitions in particular affect the dynamics of the decay of a metastable state. As it stands  $F(L)$  describes the equilibrium state for conserved order parameter  $m$ . It tells us for example whether adatoms with a given density  $\Delta m$  on a surface of size  $L^2$  form a large single crystal island or a homogenous adatom gas. For systems with conserved order parameter, like binary alloys the typical experimental setting is a rapid quench from a uniform state at high temperature into the two phase region, followed by nucleation of droplets or spinodal

decomposition. In magnetic switching experiments <sup>(38)</sup> a system with a non-conserved order parameter is driven from one equilibrium bulk state to the other by an external magnetic field  $h$  and depending on the field strength one observes two different tunneling regimes: In the stochastic regime at small fields tunneling proceeds via the nucleation of a single droplet and as the process is rare one observes large fluctuations in tunneling times, if the experiment is repeated many times. At large fields multi-droplet states dominate the intermediate configurations of the early tunneling process. The multi-droplet nature of the tunneling in this case reduces fluctuations of tunneling times. The crossover region in-between both regimes was called the dynamic spinodal <sup>(39)</sup>.

The decay of supersaturated bulk states in any case proceeds via the formation of a single droplet - or via an ensemble of several critical droplets. Let us consider a subsystem of supersaturated matter of linear extent  $\xi$  and volume  $\xi^2$  at fixed finite  $h$ , which is embedded into a larger system of finite linear size  $L$  and volume  $L^2$ . The properties of critical droplets in vicinity of the condensation phase transition determine certain aspects of the tunneling processes, which can be activated within the subsystem. Most notably and due to the existence of the condensation phase transition we observe, that volumes of critical droplets  $\Omega_{crit}$  cannot be arbitrary small for given subsystem size  $\xi$ . Their values are bounded from below through a  $\xi$  dependent bound, which is saturated at the condensation phase transition

$$\Omega_{crit} \geq \frac{1}{27m_0A_{cond}} \xi^{4/3} \quad (5.29)$$

with  $A_{cond}$  as given in Eq. (4.8). The volume of critical droplets according to Eq. (5.27) is proportional to  $h^{-2}$  and can have any value. At small values of  $h$  the critical droplet volume is large and the inequality of Eq. (5.29) is satisfied even for values  $\xi = L$ . In this region stochastic tunneling takes place with the nucleation of a single droplet. On the other hand, at large values of  $h$  the critical droplet volume is small and the inequality of Eq. (5.29) only is satisfied if  $\xi < L$ . Consequently tunneling proceeds within many subsystems of size  $\xi$  i.e., multi-droplet states are encountered. For finite size systems with linear extent  $L$  and volume  $L^2$  we determine the magnetic field  $h_{DS}$ , where the crossover from single- to multi-droplet decay takes place, as

$$h_{DS} = 2c_2A_{cond} L^{-2/3} \quad (5.30)$$

and for values  $h > h_{DS}$  we find the subsystem linear size

$$\xi(h) = \left[ \frac{2c_2A_{cond}}{h} \right]^{3/2} \quad (5.31)$$

with  $\xi(h = h_{DS}) = L$ . The interplay of the condensation phase transition with the dynamic spinodal <sup>(39)</sup> was already noted in <sup>(9)</sup>. These authors argued however in favor of a logarithmic  $L$  - dependency  $(\ln L/L)^2$  instead of the  $L^{-2/3}$  dependence of the critical field  $h_{DS}$ . Recent rigorous arguments <sup>(37,40)</sup> on the location of the condensation phase transition exclude such leading logarithmic corrections in the finite size behavior of  $F_L(m)$ . Our simulation reveals sizable sub-leading finite size corrections for the considered lattice sizes, which deserve further studies. With the assumption, that the multi-droplet physics necessary to derive the location of the dynamic spinodal is already contained in the free energy landscape of the restricted magnetization equilibrium partition function, logarithmic terms should be absent in the leading  $L$  dependence of  $h_{DS}$ . Further efforts are necessary to check, whether this assumption holds true or whether the dynamical effects invoked in <sup>(39)</sup> change the  $L$  dependence of  $h_{DS}$ .

## 6. CONCLUSION AND OUTLOOK

The constraint magnetization partition function of the 2D Ising model, which we studied at inverse temperature  $\beta = 0.7$ , hosts a variety of thermodynamic singularities, which qualify as genuine first-order phase transitions with free energy barriers, that diverge in the thermodynamic limit. The phase space on the torus splits into five disconnected sectors: bulk, droplet and strip phases (+/- symmetric states counted separately) and, on cube-surface lattices the number of phases is even higher, nine in total. On toroidal and cube-surface lattices we observe shape transitions, which strongly depend on the choice of the lattice manifold and, which for finite systems only can be avoided, if the model could be formulated on a perfect sphere. Since no such regularization is known, we are faced with discontinuous behavior for certain quantities and with free energy barriers, which are proportional to the system size  $L$ . The barrier value and the position of the crystal shape transition on the torus (from a droplet to a strip) and the positions and barriers of the “corner occupying” droplet shape transitions on the cube-surface, all are very well described by a classical droplet description.

The algorithmic performance of multicanonical ensemble simulations suffers from the existence of such shape transitions. Barriers at the discontinuous phase transitions can not be removed and result into exponential slowing down. The earlier general conjecture of random walk behavior for multicanonical ensemble simulations in applications to first-order phase transitions is falsified for a special case. This interesting algorithmic fact until now has escaped detection, just because free energy barriers in most

applications of multicanonical ensemble simulations - though present - were not particularly large. There is no doubt, that energy driven first-order phase transitions on toroidal lattices with periodic boundaries possess similar crystal shape transitions e.g., from a droplet to a strip. In higher dimensions than  $d = 2$ , e.g. in  $d = 3$ , one faces the additional fact, that two phase separation on toroidal boxes in intermediate stages also proceeds with the formation of cylinders, which adds additional shape transitions to the scenario. We expect, that the performance degradation, which is observed in multicanonical ensemble simulations, is a general property of broad histogram sampling methods for phase separated systems and, that Wang-Landau density of states updating also is affected.

For toroidal lattices we have obtained a precise finite size parameterization for droplet and strip free energies - and for the finite size energy rounding at the crystal shape transition. Our finding predicts the existence of logarithmic phase space factors in the droplet volume, which in addition to Gibbs-Thomson and capillary wave fluctuation corrections, contribute to the droplet free energy. Such terms reflect the fact, that droplets at fixed magnetization may fluctuate to any spatial position and, for the considered droplet sizes at the crystal shape transition these corrections are actually larger, than e.g. Gibbs-Thomson corrections. A Tolman correction to the classical droplet free energy could not be observed, confirming the prediction of <sup>(30)</sup> that the amplitude of this correction vanished for systems like the Ising model, which are symmetric under the interchange of the two phases. We have conjectured, that translational invariance for strip states is broken, because similar logarithmic phase space factors are absent for the strip free energy. It would be quite interesting to study the dependence of this effect on temperature and dimension.

The phase separated region of the 2D Ising model is bounded by a condensation phase transition, which as we checked at  $\beta = 0.7$  is of discontinuous nature. Within the scope of the present paper we worked out the consequences of a simple theoretical model in the one droplet sector, which is based on classical droplet theory and Gibbs-Thomson corrections. Gibbs-Thomson corrected classical droplet theory decomposes the free energy into the classical contribution of the droplet, adding fluctuations through the expansion of the Ginzburg-Landau free energy, which in this paper was considered up to second order. This theory performs surprisingly well for large droplets. The finite size condensation phase transition shift, the gap in the minority droplet size, the ratio of the shift over the gap and the nucleation barrier - all seem to approach the second order Ginzburg-Landau free energy theoretical prediction. Future studies should answer the important theoretical question, whether all of the

observed corrections for large, small and smallest droplets can be incorporated through a higher order expansion of the Ginzburg-Landau free energy, which as already mentioned requires precise knowledge on the shape of the constraint effective potential in vicinity of the bulk. We have also presented an argument relating the condensation phase transition to the location of the dynamic spinodal, which is of relevance for magnetic field switching experiments.

Thermodynamic singularities associated with the condensation of droplets in models with phase separation are expected to exist in any dimension - and also for temperature driven first-order phase transitions. To our knowledge such transitions have not yet been studied with similar methods in numerical simulations and - for most of the time - the effect has plainly been overlooked. For purposes of illustration we display in Fig. 21 the energy probability distribution function  $P(E)$  on a  $70^2$  box from <sup>(41)</sup> in the two-dimensional  $q = 20$  Potts model at the transition temperature. The conjectured positions of two asymmetric condensation phase transitions again is indicated by finite size rounded cusps. The thermodynamic properties of these transitions, like their order and their nature in terms of droplet and fluctuation degrees have not yet been studied, neither in dimension two, nor in higher dimensions.

## ACKNOWLEDGMENTS

We like to thank W. Selke for his remarks, that lead to the study of the condensation phase transition and P.A. Rikvold for a critical reading of the manuscript and many suggestions to improve it. J.H. wants to thank M.E. Fisher and R.K.P. Zia for useful discussions. T.N. acknowledges an earlier useful discussion with K. Binder.

## NOTE ADDED IN PROOF

After completion of this work we became aware of recent work on details of the condensation transition by K. Binder (Physica A **319**:99 (2003), cond-mat/0303651), K. Binder and coworkers (cond-mat/0303642) and by M. Biskup, L. Chayes and R. Kotecký (cond-mat/0302373, math.PR/0212300, math-ph/0302031).

## REFERENCES

1. K. Binder and M. H. Kalos, J. Stat. Phys. **22**:363 (1980).
2. K. Binder, Rep. Prog. Phys. **50**:783 (1987).
3. J. Richert and P. Wagner, Phys. Rep. **350**:3 (2001).

4. S. Doniach, T. Garel and H. Orland, J. Chem. Phys. **105**:1601 (1996).
5. L. Amendola et al., New Astronomy **4**:339 (1999).
6. L. S. Schulman, J. Phys. A: Math. Gen. **13**:237 (1980).
7. K. Binder, Z. Phys. B **43**:119 (1981).
8. H. Furukawa, and K. Binder, Phys. Rev. B **26**:556 (1982).
9. J. Lee, M. A. Novotny, and P. A. Rikvold, Phys. Rev. E **52**:356 (1995).
10. B. A. Berg and T. Neuhaus, Phys. Lett. B **267**:249 (1991).
11. B. A. Berg and T. Neuhaus, Phys. Rev. Lett. **68**:9 (1992).
12. B. A. Berg, U. Hansmann and T. Neuhaus, Phys. Rev. B **47**:497 (1993).
13. B. A. Berg, U. Hansmann and T. Neuhaus, Z. Phys. B **90**:229 (1993).
14. B. A. Berg, J. Stat. Phys. **82**:323 (1996).
15. F. Wang and D. P. Landau, Phys. Rev. Lett. **86**:2050 (2001).
16. T. Neuhaus, J. S. Hager preprint.
17. K. Leung and R. K. P. Zia, J. Phys. A: Math. Gen. **23**:4593 (1990).
18. M. E. Fisher, Physics **3**:255 (1967).
19. J. S. Langer, Ann. Phys. **41**:108 (1967).
20. B. McCoy and T. T. Wu, *The two-dimensional Ising-model*, Harvard University Press, Cambridge (1973).
21. C. Rottman and M. Wortis, Phys. Rep. **103**: 59 (1984)
22. G. Wulff, Z. Kristallogr. **34**:449 (1901).
23. W. L. Winterbottom, Acta Metall. **15**:303 (1967).
24. R. K. P. Zia, J. E. Avron and J. E. Taylor, J. Stat. Phys. **50**:727 (1988).
25. S. B. Shlosman, Commun. Math. Phys. **125**:81 (1989).
26. V. Privman, Phys. Rev. Lett. **61**:183 (1988).
27. M. P. Gelfand and M. E. Fisher, Int. J. Thermophys. **9**:713 (1988).
28. R. C. Tolman, J. Chem. Phys. **17**:333 (1949).
29. J. G. Kirkwood and F. P. Buff, J. Stat. Phys. **17**:338 (1949).
30. M. P. A. Fisher, and M. Wortis, Phys. Rev. B **29**:6252 (1984).
31. B. Krishnamachari, J. McLean, B. Cooper, and J. Sethna, Phys. Rev. B **54**:8899 (1996).
32. M. Pleimling and W. Selke, J. Phys. A: Math. Gen. **33**:L199 (2000).
33. M. Pleimling and A. Hüller, J. Stat. Phys. **104**:971 (2001).
34. A. Coniglio et. al., J. Phys. A: Math. Gen. **10**:205 (1977).
35. C. Borgs and R. Kotecký, Physica A **194**:128 (1993).
36. M. Campostrini, J. Stat. Phys. **103**:369 (2001).
37. T. Bodineau, D. Joffe, and Y. Velenik, J. Math. Phys. **41**:1033 (2000).
38. H. L. Richards, M. Kolesik, P. A. Lindgård, P. A. Rikvold and M. A. Novotny, Phys. Rev. B **55**:11521 (1997).
39. P. A. Rikvold, H. Tomita, S. Miyashita and S. W. Sides, Phys. Rev. E **49**:5080 (1994).
40. M. Biskup, L. Chayes, and R. Kotecký, Europhys. Lett. **60**:21 (2002).
41. A. Billoire, T. Neuhaus, and B. Berg, Nucl. Phys. **B413**:795 (1994).